JOURNAL OF MAGNETIC RESONANCE **124,** 259–262 (1997)
ARTICLE NO. MN961054

Fast NMR Imaging with B_1 Gradients

R. RAULET, D. GRANDCLAUDE, F. HUMBERT, AND D. CANET

Laboratoire de Méthodologie RMN, Université Henri Poincaré, Nancy I, B.P. 239, 54506 Vandoeuvre-lès-Nancy Cedex, France*

Received October 29, 1996

Methods aimed at obtaining an NMR image in a very short time, on the order of 1 s or less, are well established when spatial encoding is achieved by B_0 gradients. In addition to echo-planar imaging (EPI) invented by Mansfield (*1*), some other schemes have been proposed relatively recently (*2–4*). On the other hand, it has been shown that imaging by B_1 gradients (*5*) may present some advantages over B_0 gradients, especially whenever magnetic susceptibility variations are present across the object and can then cause severe distortion problems with the latter method (*6*). However, although the measuring time can be substantially reduced by acquiring the spatially encoded NMR signal between pulses of B_1 gradient (*7–9*), producing an image within a very short period is still a challenge. This may be of some interest in the context of the microscopic observation of systems evolving on a very short time scale, and ideally, one would like to devise a procedure similar to EPI, which is capable of sampling the so-called *k* space (the reciprocal space) in a single experiment. The objective of the present Communication is to demonstrate that such a capability of acquiring a 2D image in some seconds exists, and that future technological developments which could further reduce this measuring time down to the state-of-the-art of B_0 gradient imaging are anticipated.

Let us first recall how our standard imaging experiment with B_1 gradients works (*5*). A single-turn coil generates a radiofrequency field whose amplitude varies linearly across the object under investigation; we shall denote by *X* the spatial direction along which the B_1 gradient is applied. Another coil of standard design (saddle shaped) orthogonal to the gradient coil (in order to minimize leakage problems) serves merely for detection of the NMR signal. If it were possible to acquire the NMR signal during the application of the B_1 gradient, its Fourier transform would yield the projection of the spin density along the *X* direction. A set of projections for different orientations of the sample would then allow for the reconstruction of an image representative of the spin density in the *XY* plane [according to a method (*5*) derived from the filtered-back-projection algorithm (*10*)]. Because of the difficulty of rotating the gradient in this plane (this would require the implementation of a second gradient coil and would pose the problem of coupling between the three coils implemented in the probe), the experimental arrangement is such that the sample (instead of the gradient) is rotated around the *Z* axis. The point of concern is obviously the impossibility of acquiring the NMR signal while the RF gradient is on, due to the inevitable residual leakage between the gradient coil and the detection coil. For this reason, the gradient is applied in the form of short pulses with the acquisition of a single data point between two consecutive pulses, the receiver being gated on by the end of a gradient pulse and gated off again prior to the next pulse. It is easy to understand that the duration of gradient pulses determines the field-of-view and must therefore be adapted to the size of the object under examination (*5*). Finally, we purposely leave aside the problem of slice selection (along the *Z* direction of the laboratory frame), and for the sake of the present study, the object will be physically limited in thickness.

In the normal experiment, each projection, acquired for a given object orientation, is followed by a waiting time which allows for the spin system to return to thermal equilibrium before the next sample rotation. Owing to the fact that about a hundred projections are necessary for obtaining an image of good quality, a typical measuring time is on the order of 10 min. The idea for lowering this waiting time is that

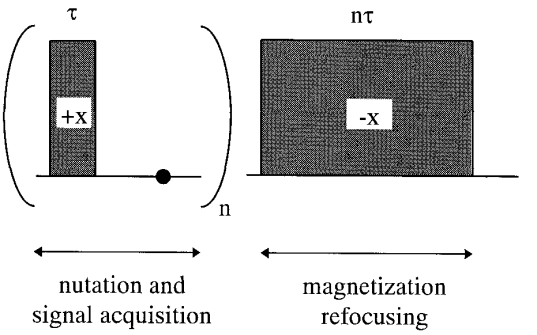

FIG. 1. The basic scheme of the fast imaging method with B_1 gradients. Each of the *n* elements in the loop includes a short B_1-gradient pulse (of duration τ) followed by the acquisition of a single data point (dot). Refocusing is produced by a long B_1-gradient pulse (of duration $n\tau$), whose phase is opposite to the phase of RF pulses in the loop.

* URA CNRS 406-LESOC; FU CNRS E008-INCM.

1090-7807/97 $25.00

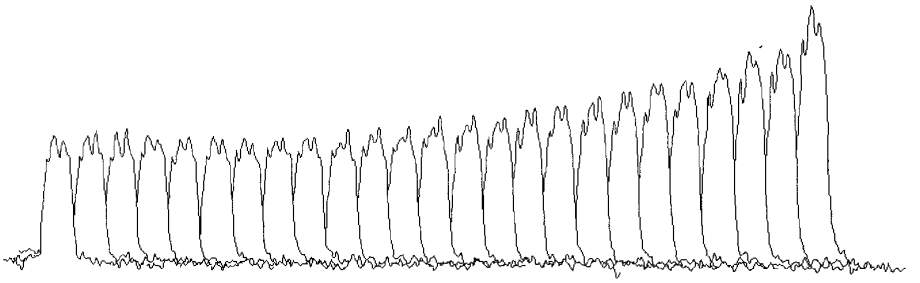

FIG. 2. A series of profiles resulting from the space-encoding–refocusing process of Fig. 1 (without sample rotation), which shows the establishment of a steady state. The time elapsed between two consecutive cycles is 50 ms. Each profile is obtained with 128 B_1-gradient pulses of 25 μs duration separated by 20 μs acquisition windows (gradient strength: approximately 2 G/cm).

magnetization defocusing (with respect to the axis of the rotating frame along which the B_1 gradient is applied, say x), which provides space encoding, is reversible. Let us suppose that we have applied n B_1-gradient pulses of duration τ for encoding purposes, starting from nuclear magnetization along the z axis (in its equilibrium state), and disregarding for the moment relaxation phenomena, we can see that magnetization can be taken back to the z axis provided that a long B_1-gradient pulse of duration $n\tau$ is applied along the $-x$ axis of the rotating frame. This is illustrated in Fig. 1. In fact, because the pulses in the train are not perfectly rectangular, the long refocusing pulse must be adjusted in length: with the present experimental setup and for a typical set of 128 pulses of 25 μs duration, the best refocusing is obtained with a long pulse of 3.27 ms duration instead of the expected 3.20 ms.

We now must account for relaxation phenomena which manifest themselves during the application of the train of B_1-gradient pulses as well as during the long refocusing pulse. Under nutation (for instance, in the yz plane, produced by a radiofrequency field acting along the x axis of the rotating frame), nuclear magnetization decays according to a relaxation time $T_{1,2}$ such as $1/T_{1/2} = (1/2)(1/T_1 + 1/T_2)$, whereas the decay is governed by T_2^* during acquisition windows [although, in that latter situation, partial refocusing effects occur (5)]. Nevertheless, signal losses are expected in the course of successive defocusing (spatial encoding)–refocusing processes, and because of the repetitive nature of the experiment, one may hope to reach a stationary state. This is indeed verified by the series of profiles shown in Fig. 2 which have been obtained under the experimental conditions indicated above; this unfortunately entails a sensitivity loss by about a factor of 2. In order to produce an image devoid of intensity distortions, it is therefore recom-

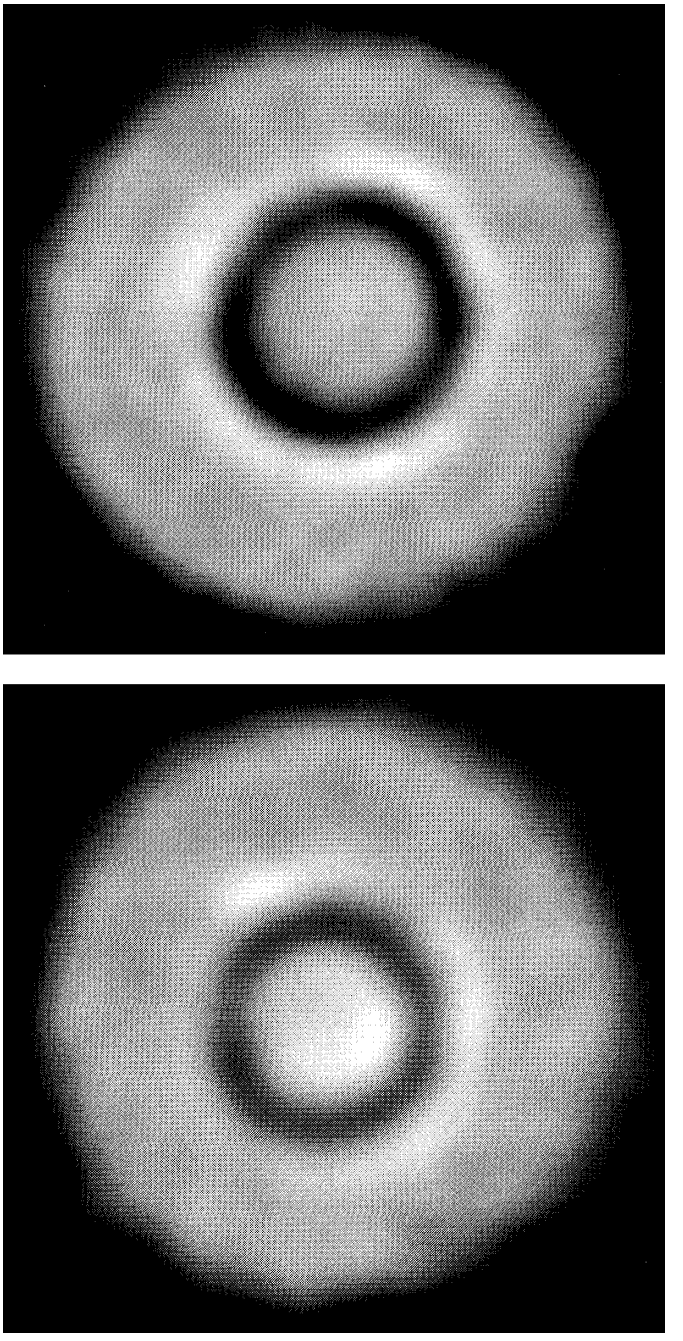

FIG. 3. Images of the phantom described in the text, each one resulting from 100 projections (one scan) with an angular increment of 3.6°. In each case, 28 dummy scans were run. (Top) Normal experiment (without refocusing); total duration, 10 minutes. (Bottom) Fast experiment (with refocusing, 50 ms between two consecutive cycles); total duration, 6 s. Other experimental parameters are given in the legend to Fig. 2.

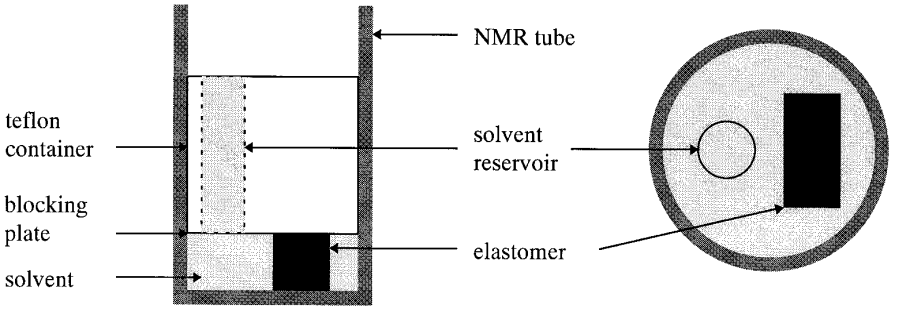

FIG. 4. The device used to study solvent penetration into an elastomer sample designed for maintaining the polymer surface in contact with the solvent. Sample height: 1 mm. NMR tube internal diameter: 3 mm.

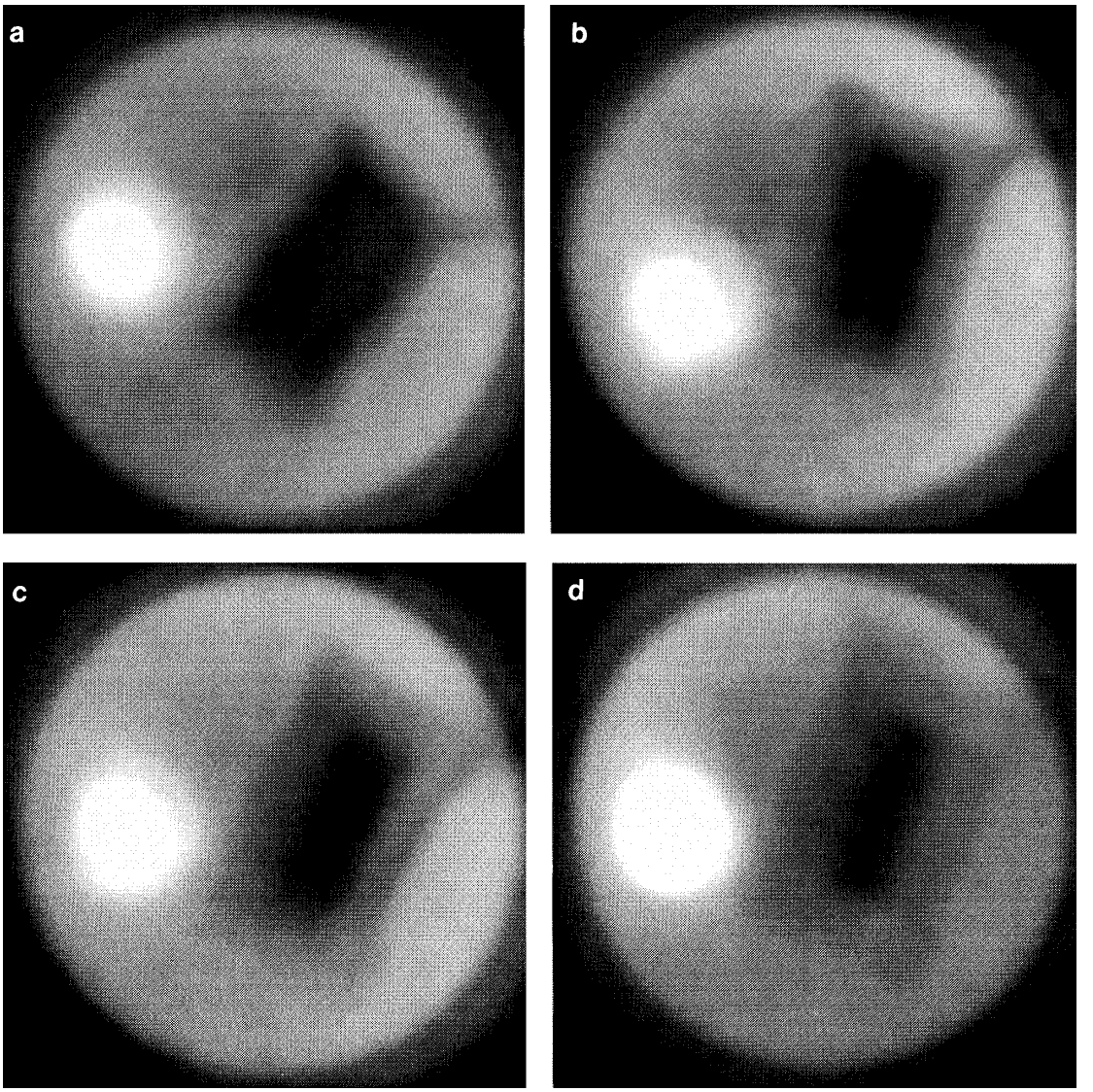

FIG. 5. A series of images showing the penetration of isooctane into an elastomer sample; each image is obtained by the fast procedure respectively at 2 (a), 7 (b), 12 (c), and 17 min (d) after immersion (the device shown in Fig. 4 and the experimental conditions described in the legend to Fig. 3 were used).

mended to perform a series of dummy defocusing–refocusing processes until one arrives at the steady state and, of course, to discard these dummy experiments in the image reconstruction.

Another issue is the rotation of the sample which could be accomplished by a stepping motor. However, this would entail a nonnegligible time interval at each new step. For this reason, we concluded that it was better to rotate the sample continuously, accepting the slight error in the angle associated with a given projection. With the standard experimental conditions of this work, this represents at most an error of 0.3°, presumably quite tolerable with respect to the expected spatial resolution.

Last, but not least, we still must face the problem of probe overheating due to the almost constant application of radiofrequency pulses. The major drawback is a detuning of the gradient coil which results in a lowering of the gradient strength and thus in shifted profiles. A way of circumventing this problem is to evacuate the heat in excess by an air flow cooled at an appropriate temperature before being injected into the probe. Although, with this simple remedy, the time between two consecutive defocusing–refocusing cycles could be reduced to 50 ms, this remains the critical feature (and hopefully improvable) of the method.

A first test was carried out with a phantom consisting of a 1 mm o.d. glass capillary centered in a cylindrical Teflon container of 3 mm o.d. Some water was placed inside and outside the capillary so that the liquid height did not exceed 1 mm in order to avoid the implementation of a slice-selection procedure. However, because of meniscus and wetting problems, the water column height is far from being uniform as seen in the images of Fig. 3. This figure compares the results obtained with the normal and fast procedures, respectively, and demonstrates the reliability of the latter.

The next example deals with solvent penetration into polymeric materials. NMR imaging (or microscopy) constitute a promising technique for such physicochemical studies (*11*) but until now has been applied to systems for which solvent penetration is slow, leaving plenty of time for performing the NMR imaging experiment. We address here the problem of systems for which the usual measuring time (i.e., 10 min) becomes important with respect to the rate of the uptake process. This is the case of a particular elastomer (Fig. 5) highly permeable to isooctane. A special device, shown in Fig. 4, has been used; it has been designed so that, regardless of swelling phenomena and solvent uptake, the elastomer is always immersed in the solvent. The results, displayed in Fig. 5, fully justify the recourse to a fast microscopy procedure, as after 17 min, half of the elastomer sample has been imbibed with solvent. It may be noted that, despite the huge signal arising from the reservoir (with some distortion for this signal due to the lack of slice selection), details in the elastomer image, including the diffusion front and swelling, are perfectly visible. Of course, the spatial resolution is not at its best. In particular, recent instrumental improvements leading to much stronger gradients (*12*) have not been implemented because we prefer to avoid further temperature problems and are awaiting a more dedicated probe. Another reason may be the slight inaccuracy due to the continuous rotation of the sample (see above).

We hope to have demonstrated the potentialities of the fast imaging method presented in this paper, and its interest for the study of objects in rapid evolution. We believe that improvements in the probe design, directed especially to a more efficient temperature control, should allow us to further reduce the measuring time.

REFERENCES

1. P. Mansfield, *J. Phys. C.* **10,** L55 (1977).
2. A. Haase, *Magn. Reson. Med.* **13,** 77 (1990).
3. D. Norris, *Magn. Reson. Med.* **17,** 539 (1991).
4. J. Hennig and M. Hodapp, *Magma* **1,** 39 (1993).
5. P. Maffei, P. Mutzenhardt, A. Retournard, B. Diter, R. Raulet, J. Brondeau, and D. Canet, *J. Magn. Reson. A* **107,** 239 (1994).
6. R. Raulet, J.-M. Escanyé, F. Humbert, and D. Canet, *J. Magn. Reson. A* **119,** 111 (1996).
7. D. Boudot, D. Canet, and J. Brondeau, *J. Magn. Reson.* **87,** 385 (1990).
8. K. R. Metz, J. P. Boehmer, J. L. Bowers, and J. R. Moore, *J. Magn. Reson. B* **103,** 152 (1994).
9. J. L. Bowers, P. M. MacDonald, and K. R. Metz, *J. Magn. Reson. B* **106,** 72 (1995).
10. P. T. Callaghan, ''Principles of Nuclear Magnetic Resonance Microscopy,'' Clarendon Press, Oxford, 1991.
11. M. A. Rana and J.-L. Koenig, *Macromolecules* **27,** 3727 (1994); M. Ilg, B. Pfleiderer, K. Albert, W. Rapp, and E. Bayer, *Macromolecules* **27,** 2778 (1994); M. Valtier, P. Tekely, L. Kiéné, and D. Canet, *Macromolecules* **28,** 4075 (1995).
12. F. Humbert, B. Diter, and D. Canet, *J. Magn. Reson. A* **123,** 242 (1996).